Aerosol jet fog (ajFOG) deposition of aluminum oxide phosphate thin films from an aqueous fog

Nishit M. Murari
School of Electrical Engineering and Computer Science, Oregon State University, Corvallis, Oregon 97331-5501, USA

Ryan H. Mansergh and Yu Huang
Department of Chemistry, Oregon State University, Corvallis, Oregon 97331-4003, USA

Matthew G. Kast
Department of Chemistry and Biochemistry, University of Oregon, Eugene, Oregon 97403-1253, USA

Douglas A. Keszler
Department of Chemistry, Oregon State University, Corvallis, Oregon 97331-4003, USA

John F. Conley Jr.[a]
School of Electrical Engineering and Computer Science, Oregon State University, Corvallis, Oregon 97331-5501, USA

A new lab-based aerosol jet fog (ajFOG) deposition system with an atomizer consisting of two opposing jets located within the deposition chamber is introduced and its capabilities are examined. The unique opposing configuration of the atomizer enables the formation of a highly uniform fog even from low volatility precursors. Aluminum oxide phosphate (AlPO) thin films were deposited onto Si wafers at room temperature and sub-atmospheric pressure by using an aqueous precursor. Films were characterized by spectroscopic ellipsometry, x-ray diffraction and reflectivity, scanning electron microscopy, and metal/oxide/semiconductor (MOS) capacitor electrical measurements. Film thickness uniformity, density, surface roughness, and charge transport mechanisms were found to be comparable to spin-coated thin films deposited using the same precursor, demonstrating the effectiveness of this aerosol technique. A process model was developed to predict film thickness as a function of precursor concentration, exposure time, fog settling time, and number of exposures.

I. INTRODUCTION

In this work, we introduce a new lab-based aerosol jet fog (ajFOG) deposition system by producing and validating high-quality aluminum oxide phosphate films. We show that uniform films are readily deposited from a homogeneous fog at room temperature and pressure. The semiconductor, glass, and solar industries have historically relied on vacuum deposition to produce uniform thin films on various flat and textured substrates.[1] As these industries explore and introduce new technologies, opportunities arise to consider new cost-effective, environment friendly, and less energy intensive deposition techniques, especially to address scaling issues. Solution-based spin coating, for example, satisfies most needs and produces high quality organic and inorganic thin films,[2] but physical limitations restrict its use to modest substrate sizes.[3,4] Lately, researchers have

been addressing spin coating constraints by investigating aerosol techniques such as spray coating,[5] spray pyrolysis,[6] mist chemical vapor deposition (MCVD),[7] and liquid source misted chemical deposition (LSMCD).[8] These techniques aim to initially produce homogeneous aerosols of volatile molecules, liquids, or solutions[9,10] that then deposit to form uniform films, potentially over large areas. Among aerosol methods, LSMCD so far produces the most uniform and smoothest films, but its complexity makes scaling substrates to large sizes unlikely.[11]

To examine the potential of aerosol deposition to produce uniform films from a homogeneous fog and enable new capabilities, we have worked with Beneq Corporation to design a laboratory deposition system. The ajFOG system employs a novel atomizer consisting of two opposing jets located inside the deposition chamber. Head on collision of the opposing jets shears precursor droplets into a fine mist or fog that uniformly fills the deposition chamber and enables the use of low volatility precursors. We explore system capabilities by studying deposition of aluminum oxide phosphate (AlPO) thin films from an aqueous precursor. AlPO has

---

received considerable attention for applications requiring abrasion resistance, chemical resistance, low refractive index, and low electrical leakage.[12–14] AlPO has previously been deposited via spin coating[12,13] and atomic layer deposition.[14] Here, we develop a model to predict AlPO film thickness as a function of ajFOG process variables; precursor concentration, fog settling time, fog exposure time, and number of coating cycles. ajFOG and spin-coated films are compared side-by-side by using spectroscopic ellipsometry (SE), x-ray reflectivity (XRR) and diffraction (XRD), and metal/oxide/semiconductor (MOS) capacitor measurements to highlight the effectiveness of the ajFOG method.

II. EXPERIMENTAL

A. Precursor preparation

The aqueous aluminum phosphate-based (AlPO) hetero-polycation precursor with the general formula $Al_5O_3(PO_4)_3$ is synthesized using aluminum nitrate (98% Sigma Aldrich), nitric acid (99.9% Alfa Aesar), and deionized water (18.2 $M\Omega$). Final precursor solutions were diluted to desired concentrations and filtered with a 0.2-μm polytetrafluoroethylene (PTFE) filter. A detailed description of the preparation of AlPO precursor has been reported previously.[13]

B. Thin film deposition

Aqueous AlPO precursors were deposited onto 150-mm Si wafers via both ajFOG deposition and spin coating to form $Al_5O_3(PO_4)_3$ thin films. Prior to thin film deposition, silicon substrates were cleaned using acetone, isopropanol, and deionized water for 10 min each in ultrasonic bath followed by a 10 min UV ozone treatment.

The Beneq ACS 200-101 aerosol jet fog (ajFOG) deposition system (Beneq, Espoo, Finland) produces a fog at room temperature and slightly below atmospheric pressure via a novel atomizer. Figure 1 shows a simplified schematic of the ajFOG system. (A labeled photograph of the actual system is shown in Fig. S1.) Two independent

aerosol nozzles, directed one to the other, form the atomizer. Dosing diaphragm pumps supply each nozzle with precursor solutions to produce high-velocity jets of fine precursor droplets. These droplets collide head-on and shear into smaller sizes to produce a flat and evenly distributed aerosol disc [Fig. 1(b)]. Over time, momentum carries the droplets throughout the chamber to create a homogeneous fog. Uniform aerosol fog generation via droplet collision is a unique aspect of the system. Precursors may be fed independently to each nozzle; in this work, the aqueous AlPO precursor was supplied to each nozzle. The substrate is introduced into the chamber via a load lock, which is kept at a slightly positive pressure with respect to the chamber, preventing aerosol fog from leaking into the load lock. $N_2(g)$ flows through Venturi vacuum generators to create a slight vacuum and contain the aerosol fog within the deposition chamber.

Films may be deposited either in continuous mode or pulse mode. In continuous mode, the substrate is introduced into the chamber while the aerosol fog is continuously generated. As soon as the aerosol fog droplets contact the substrate, they spread completely due to the UV-ozone treated substrate's high-surface energy. The exposure time and the interaction energy between the droplets and the surface determine the equilibrium film thickness.[15]

In pulse mode, aerosol generation is interrupted, allowing fog droplets to stabilize inside the chamber for a selected wait time, t_w, before introducing the substrate. Visually, fog density decreases over time as droplets gradually settle at the bottom of the chamber due to gravity; after about 600 s, the fog has dissipated completely. The wait period produces a uniform fog of small droplets, as large droplets settle first due to gravity [consider Fig. 1(c)]. While we have not measured the average droplet size in the fog, their persistence in the chamber indicates a radius smaller than the capillary length $\lambda_c = [(\gamma/\rho g)]^{1/2}$, where γ is surface tension, ρ is density, and g is gravity.[16] Assuming droplet density and surface tension equivalent to those of water, the maximum droplet diameter after initial settling should be
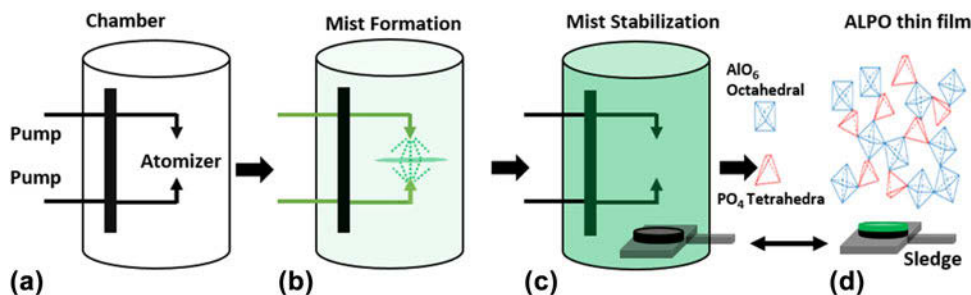

FIG. 1. Operational schematic of the ajFOG deposition system at different stages: (a) deposition chamber, (b) formation of aerosol by 180° impact of opposing precursor jet streams, (c) uniform mist after stabilization and introduction of substrate, and (d) removal of substrate by sledge after thin film deposition. Also shown in (d) is a schematic of the AlPO thin film structure.

approximately 10 μm or smaller. In this work, films were deposited in pulse mode, typically with t_w = 120 s.

After a prescribed exposure time, t_{exp}, of the substrate in the chamber the coated substrate is transferred from the chamber to the load lock. To prevent rapid film drying and to promote spreading and uniformity, the load lock is supplied with moist $N_2(g)$. The coated substrate rests in the load lock for a set "leveling" time, allowing the droplets to coalesce and form a continuous film [see Fig. 1(d)].[17,18] The minimum leveling time in this work is 30 s; shorter times compromised film uniformity. When higher precursor concentration solutions are used, longer leveling times are needed. When removed from the chamber, the film is initially wet and susceptible to air turbulence. If the load lock is opened too early, air turbulence produces uneven drying across the wafer, decreasing uniformity. During the leveling period, a gradually receding rainbow pattern indicates film thickness is changing consistent with drying. After leveling, the coated substrate is removed from the load lock and cured on a hotplate at 300 °C for 1 min prior to any analysis. A complete deposition cycle—fog formation, leveling, and exposure—requires approximately 10 min. Finally, 18.2-MΩ deionized water is run through the nozzles after each deposition to purge residual precursor.

For comparison studies, the same aerosol precursor solutions were spin coated onto Si substrates at 3000 rpm for 30 s, then cured at 300 °C for 1 min on a hotplate.

C. Thin film characterization

AlPO films were analyzed either after the 300 °C cure, or following anneals in a Eurotherm box furnace at 300, 400, 500, and 800 °C for 1 h in air. Spectroscopic ellipsometry (SE) was conducted using a J.A. Woollam, Inc., (Lincoln, Nebraska) M-2000 instrument. Thirty-seven point thickness maps were measured at incident angles of 60 and 65° in the wave length range 370–1000 nm. A Cauchy model fitting of Ψ and Δ with respect to wave length was used to extract film thickness and refractive index.

X-ray reflectivity (XRR) and diffraction (XRD) data were collected with a Rigaku Ultima-IV (Rigaku Corporation, Tokyo, Japan) x-ray diffractometer equipped with Cu K$_\alpha$ radiation (λ = 1.5409 Å) and configured with 5.0° incident and receiving Soller slits and a 10-mm divergent height limiting slit. Data modeling was performed with Rigaku GlobalFit modeling software[19,20] using a four layer model consisting of the substrate, the substrate-AlPO interface, the AlPO film, and a surface crust.

For electrical characterization, circular, 250-μm diameter aluminum dots were thermally evaporated through a shadow mask to form the top electrodes. Capacitance versus voltage (C–V) and current versus voltage (I–V) measurements were carried out on a probe station in a dark box at room temperature using an Agilent 4284A Precision LCR meter and an Agilent (Santa Rosa, California) 4155C Semiconductor Parameter Analyzer, respectively. Si p-type (1.5 Ω-cm) substrates were used for C–V measurements while Si n-type (0.0010–0.0055 Ω-cm) substrates were used for I–V measurements. The Si substrates constituted the bottom electrodes and were held at ground. The ideal flatband voltage, $V_{FB\text{-}ideal}$, was calculated from the work-function difference between the aluminum electrode and the semiconductor substrate, assuming Φ_{Al} = 4.1 eV and acceptor doping of $10^{16}/cm^3$. Experimentally determined V_{FB} were determined using the inverse 2nd derivative method described by Schroeder.[21]

III. RESULTS AND DISCUSSION

A. Thickness and uniformity

Figure 2(a) shows a thickness contour map for an ajFOG deposited film cured at 300 °C. Film thickness varies between 13.5 and 14.5 nm with the mean = 14.1 nm; thickness varies by less than 4% across the 150-mm wafer. As an aqueous precursor, AlPO uniformly coats hydrophilic surfaces. A 10-min ultraviolet (UV) ozone treatment prior to deposition produces a uniformly hydrophilic surface. A shorter UV ozone exposure time is insufficient as surface-energy discontinuities across the substrate directly influence film uniformity and quality (see supplementary Fig. S2). Small differences in chamber and load-lock pressures can create turbulence and disturb the fog distribution when the wafer moves from the chamber to the load lock. If the sample is not carefully removed, air flow during this movement can thin the leading edge of the wafer (see supplementary Fig. S3).

Figure 2(b) shows a thickness contour map of a standard spin coated film. Film thickness varies between 16 and 20 nm with the mean = 18.2 nm; thickness varies by approximately 10% over the 150-mm wafer. Comparing Figs. 2(a) and 2(b), the spin-coated films are approximately 5 nm thicker than the aerosol-deposited films and slightly less uniform. The sharp variation in film thickness at the wafer center and edge are due to the wafer chuck and edge effects, common defects associated with spin coating that are not observed in the ajFOG-deposited films.

Figure 2(c) shows refractive index and average thickness for ajFOG and spin-coated films as a function of annealing temperature. The refractive index and thickness vary in similar ways for the two deposition methods as temperature increases. At each temperature, refractive indexes differ by less than 5%. The minimum thickness for both deposition methods occurs at 500 °C, which is associated with nearly complete dehydration of the films.[22] Film thickness increases in each case at 800 °C. As 800 °C is several hundred degrees below the film crystallization temperature, as determined by XRD,[23] grain growth and coarsening do not contribute to

the increased roughness. However, the interfacial SiO_2 layer between the Si substrate and the AlPO film is likely growing at high temperatures. The similarity of the optical refractive indexes for AlPO and a growing SiO_2 layer may account for the apparent AlPO thickness increase. This SiO_2 growth requires further study.

B. Process variables

For spin coating, spin speed, spin time, and number of coatings are commonly varied to adjust and control film thickness. To control film thickness with ajFOG deposition, we have investigated the solution precursor concentration [N], exposure time (t_{exp}), wait time (t_w), intrinsic fog settling time, τ, for the system, and number of coating cycles. Figure 3(a) shows a plot of film thickness, d_{ox}, versus AlPO precursor concentration for a fixed $t_w = 120$ s and $t_{exp} = 120$ s. Film thicknesses increase from 4.3 to 90 nm by changing [N] from 0.04 to 1.0 M. Empirically, d_{ox} depends linearly on the [N] according to Eq. (1)

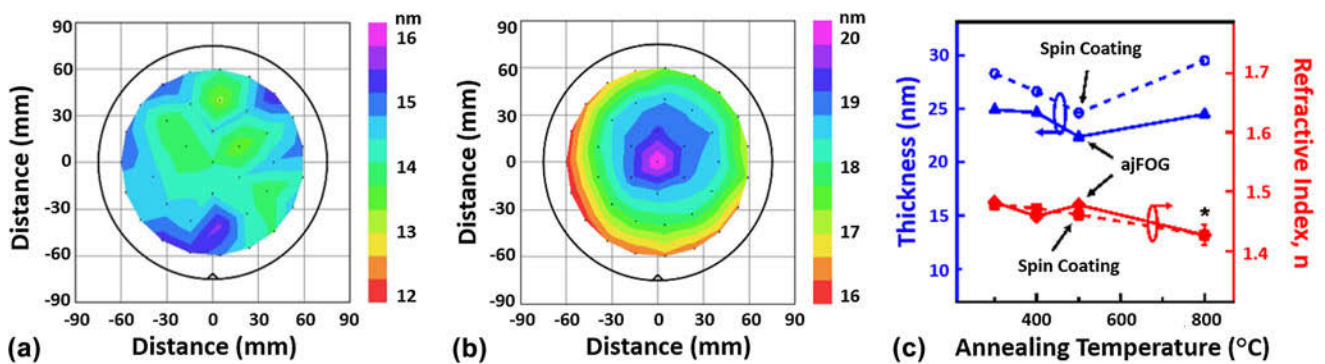$$d_{ox} = C(t_w = 120\,\text{s},\ t_{exp} = 120\,\text{s}) * [N]\quad,\qquad (1)$$

FIG. 2. Ellipsometry thickness maps of (a) ajFOG deposited and (b) spin coated AlPO thin films over a 150 mm silicon substrate following a 1 min cure at 300 °C. (c) Thickness (blue) and refractive index (red) of ajFOG (dashed lines) and spin coated (solid lines) for films as-deposited and annealed at either 400, 500, or 800 °C. The error bar indicated with an asterisk (*) is associated with the 800 °C spin coated films.
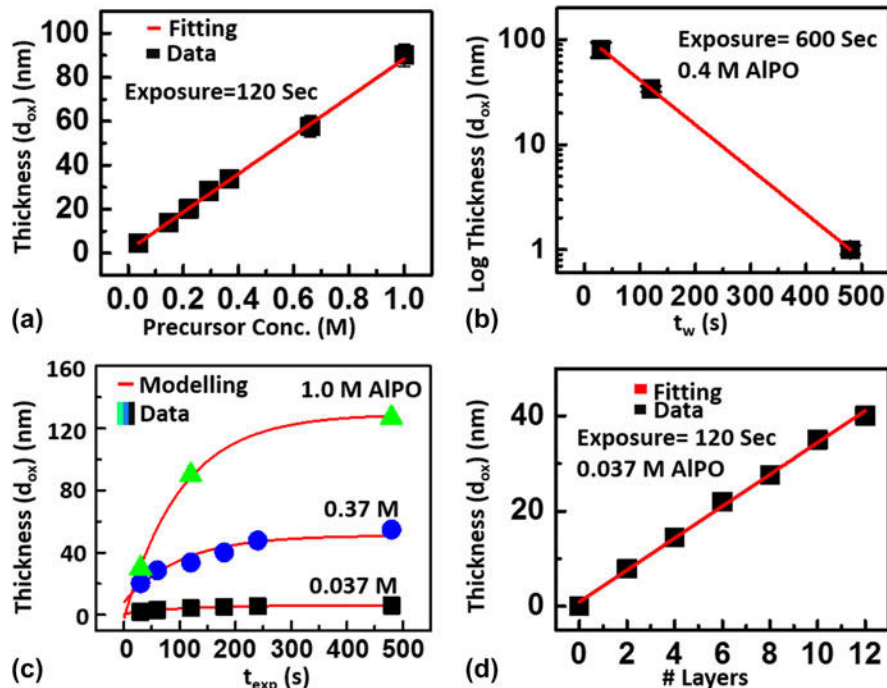

FIG. 3. (a) Variation of AlPO film thickness with precursor concentration. The red line [fit by Eq. (1)] indicates a linear dependence. (b) Log (thickness) as a function of wait time, t_w, for a fixed exposure time of 600 s, fit (red lines) by Eq. (2). (c) Thickness as a function of exposure time, t_{exp}, modeled (red lines) by Eq. (3). (d) Multilayer deposition of thin films from 0.037 M precursor. Fitting (red line) indicates linear dependence. In all plots, error bars are smaller than the symbol size. All films were as deposited and cured at 300 °C for 1 min on a hot plate.

where C(120,120) = 88 nm/M and [N] = molarity of Al in the precursor solution; C varies with t_w and t_{exp}.

In pulse mode, where the aerosol fog generation is stopped prior to exposing the substrate, the ajFOG deposition process is driven by gravity induced settling of the fog. This is observed visually to occur over a period of approximately 600 s. To evaluate the intrinsic fog settling time, τ, as well as the expected wait time (t_w) dependent saturation thickness, d_{sat}, a series of films were deposited by fixing t_{exp} and varying t_w, the amount of time that lapses between stopping fog generation and inserting the wafer into the chamber. As the chamber is fog free in less than 600 s, t_{exp} was fixed to 600 s to ensure a saturated deposition. Figure 3(b) shows a plot of $\log(d_{sat})$ versus t_w for [N] = 0.4 M. Physically, longer t_w allows more settling of the fog, in turn producing thinner films. Equation (2) describes this empirical relationship in exponential form:

$$d_{sat}([N], t_w) = d_{sat}([N], 0)\ \exp(-t_w/\tau)\quad,\qquad(2)$$

where $d_{sat}([N], t_w)$ is the saturation thickness at $t_{exp} = 600$ s as a function of [N] and t_w, $d_{sat}([N], 0)$ is the extrapolated saturation thickness at $t_w = 0$ as a function of [N], and τ is the intrinsic fog settling time for the system. The system fog settling time of $\tau \sim 102$ s is obtained by fitting Eq. (2) to Fig. 3(b).

The data from Fig. 3(b) is replotted on a linear scale in supplementary Fig. S4 with visible error bars representing the standard deviation obtained during the ellipsometry thickness mapping (37 points). If the standard deviation can be assumed to be related to the roughness then it can be inferred that the surface roughness decreases with increasing t_w. The physical basis for this is that as soon as the fog formation is stopped in the deposition chamber, the bigger and heavier droplets fall faster (due to reduced influence of Brownian forces) leaving smaller droplets suspended in the chamber. A shorter t_w allows the wafer surface to be exposed to a greater density of larger droplets, creating a rougher surface with larger thickness variation.

Next the impact of fog exposure time, t_{exp}, is investigated. Figure 3(c) shows plots of d_{ox} as a function of t_{exp} for 0.037, 0.40, and 1.0 M concentration precursor solutions at fixed $t_w = 120$ s. As seen in Fig. 3 (c), the deposition rate is directly related to the amount of fog remaining in the chamber. At short exposure times, film thickness increases rapidly with t_{exp}, slowing as the fog settles out and eventually saturating at long t_{exp}. The saturation thickness, d_{sat}, for each concentration is consistent with the results presented in Fig. 3(a). Equation (3) models film thickness as a function of t_{exp}:

$$d_{ox} = d_{sat}([N], t_w = 120)\big(1 - \exp(-t_{exp}/\tau)\big)\quad,\quad(3)$$

where $d_{sat}([N], t_w = 120)$ is the saturation thickness for a selected precursor concentration with $t_w = 120$ s and τ is the fog settling time of ~ 102 s as determined above.

Equation (3) fits well the growth profiles in Fig. 3(c), yielding $R^2 = 0.999$. Summarized in Table I are fitted $d_{sat}([N], 120)$ for the three measured precursor concentrations. $d_{sat}([N], 120)$ increases linearly with [N], consistent with Fig. 3(a) and Eq. (1). Saturation thickness, d_{sat} occurs at a fixed time, independent of the solution concentration. The close agreement of Eq. (3) with the data in Fig. 3(c) is a further indication that the fog settling time τ is an intrinsic characteristic of the ajFOG chamber with an aqueous fog.

A general equation for thin film growth can be formed by combining Eqs. (1)–(3) to arrive at

$$d_{ox} = C_{sat} \cdot [N] \cdot \exp(-t_w/\tau) \cdot \big(1 - \exp(-t_{exp}/\tau)\big)\quad,$$

$$(4)$$

where $C_{sat} = 420$ nm/M for $t_w = 0$ and $t_{exp} = \infty$. Note that C_{sat} will depend on the specific precursor used. To summarize the physical significance of Eqs. (1)–(4), ajFOG deposition depends linearly on the concentration of the precursor solution [N] in the fog droplets; on the amount of precursor fog remaining in the chamber [which decreases characteristically (τ) with wait time, t_w, and exposure time], the time the substrate spends exposed to the fog, t_{exp}, and the intrinsic settling time of the fog in the chamber (τ).

Finally, in addition to adjusting [N], t_w, and t_{exp}, the thickness may also be controlled via multiple coatings. Figure 3(d) shows a plot of film thickness versus number of coating cycles for the precursor concentration of 0.037 M. Each coating cycle was performed with $t_w = 120$ s and $t_{exp} = 120$ s followed by curing for 1 min at 300 °C. The linear dependence of thickness on the number of coating cycles shows that multiple coatings can readily produce a desired target thickness, and it also confirms the coating process is stable and reproducible. Twelve coating cycles produce a film with a thickness of roughly 40 nm, indicating that a 3.35-nm thick layer forms in each cycle.

TABLE I. Fitting constants for different precursor concentrations obtained from Eq. (3) for $t_w = 120$ s and $t_{exp} = 120$ s.

[N] (M)	$d_{sat([N],120)}$ (nm)
0.037	5.3
0.37	53.3
1.0	132.9

C. Density, surface roughness, and morphology

Figure 4 shows plots of log (XRR intensity) versus angle 2θ for (a) aerosol and (b) spin-coated films annealed for 1 h in air at the indicated temperatures. Critical angles and Kiessig fringe amplitudes are comparable for the two deposition methods, representing the extreme surface smoothness. Figure 4(c) shows derived densities for the two deposition methods. They are similar, $\sim$2.7 g/cm^3, and essentially independent of anneal temperature above 300 °C. The largest difference, 7%, between the two techniques occurs at 300 °C. Considering the variable film water content observed at this temperature, the difference is not unexpected.

Figure 4(c) shows surface roughness estimates from XRR data plotted as a function of anneal temperature. Both aerosol deposition and spin coating produce ultra-smooth surfaces with root-mean-square surface

roughness (R_q) below 0.4 nm. Values differ by less than 0.1 nm and are largely temperature independent for the two deposition methods.

Shown in Fig. 5 are (a) XRD intensity versus 2θ for 45 nm thick ajFOG and spin coated films, and (b) a plan view SEM images of the ajFOG deposited film. Taken together, the absence of any sharp peaks in the XRD spectrum, the absence of features in the SEM image, and the low surface roughness [Fig. 4(c)] are strong indications of the amorphous nature of the AlPO films.

D. Carrier dynamics

Shown in Fig. 6 is a plot of current versus electric field, E_{ox}, for (a) ajFOG deposited and (b) spin coated Al/AlPO/Si MOS devices, both as-deposited (and cured at 300 °C for 1 min) and as a function of anneal temperature. The average ellipsometric thickness of the ajFOG deposited and spin coated films were 24 and 18 nm,
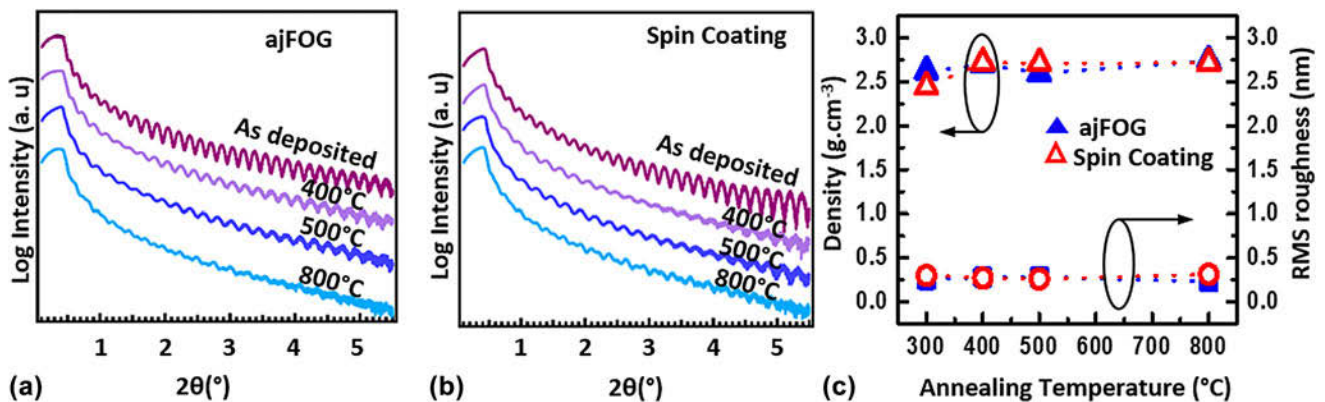

FIG. 4. XRR intensity versus angle 2θ of (a) ajFOG deposited (b) spin coated AlPO thin films on silicon substrates. (c) Density and RMS roughness of the ajFOG deposited and spin coated AlPO thin films versus anneal temperature. All films are single layer depositions with $[N] = 0.4$ M, with $t_w = 120$ s and $t_{exp} = 120$ s for the ajFOG depositions.

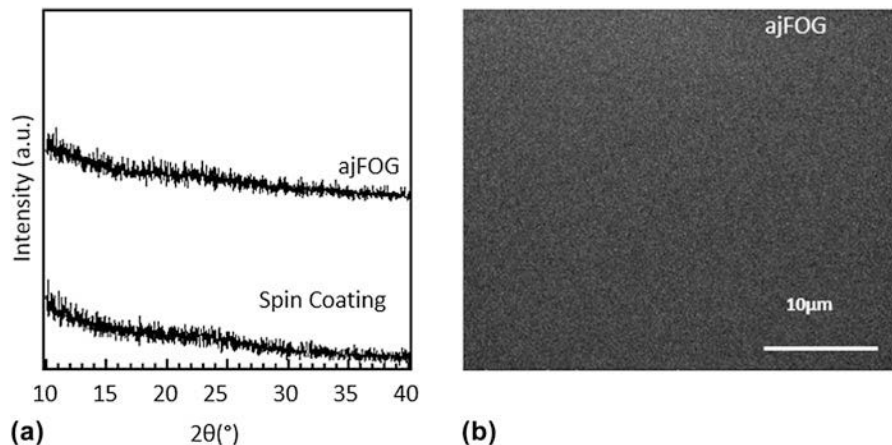FIG. 5. (a) XRD intensity versus 2θ for 45 nm thick ajFOG deposited and spin coated AlPO films. (b) Plan view SEM image of the same ajFOG film. All films were deposited using 0.4 M AlPO precursor and annealed at 800 °C for 1 h in air. The absence of any sharp peaks in the XRD pattern as well as the smooth surface and absence of features in the SEM image combined with low surface roughness [Fig. 4(c)] are strong indications of the amorphous nature of the film.
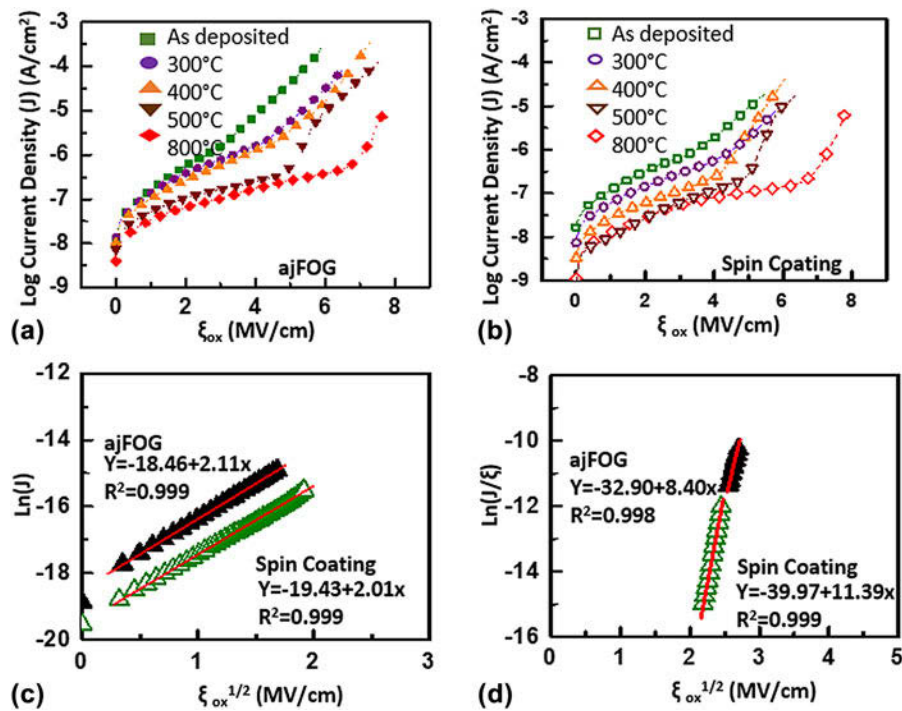
FIG. 6. Log (current density) versus electric field, ξ_{OX}, for AlPO thin film devices, as-deposited and annealed at 300, 400, 500, and 800 °C, for (a) ajFOG deposition (solid symbols) and (b) spin coating (open symbols). For a representative 400 °C annealed sample, (c) Schottky emission (ln J versus $\xi_{ox}^{1/2}$) dominates at lower applied fields, while (d) Frenkel-Poole conduction (ln J/ξ_{ox} versus $\xi_{ox}^{1/2}$) is observed at higher fields. All films are single layer depositions with $[N] = 0.4$ M, with $t_w = t_{exp} = 120$ s for the ajFOG depositions.

respectively. The electric field is calculated from the applied voltage, V, divided by d_{ox} ($\xi_{ox} = V/d_{ox}$), where d_{ox} is the ellipsometric thickness of the overall dielectric stack (which consists of the main AlPO layer, d_{AlPO}, and an interfacial layer, d_{IL}, at the substrate-AlPO interface, $d_{ox} = d_{AlPO} + d_{IL}$). The anneal temperature dependence of the J–ξ characteristics exhibited by the films is qualitatively the same, in that leakage current decreases with annealing temperature for both deposition techniques. The decrease in leakage current with increased anneal temperature is likely due to film dehydration and interfacial SiO_2 layer growth at the higher temperatures.[24,25] Similar behavior was reported in spin coated Al_2O_3 films which, in addition to decreased leakage, also showed a reduction in overall dielectric constant with increasing anneal temperature. The improvement in electrical properties was determined to be due to dehydration and the formation of a wide band gap SiO_2 interfacial layer.[26] Interfacial layer growth in the ajFOG deposited films is currently being investigated further.

The dominant mechanisms of charge transport through a dielectric can be a sensitive indication of film quality. Although Fowler-Nordheim tunneling (FNT) based conduction is desired, charge transport in high electron affinity, low temperature deposited dielectrics is commonly dominated by either "bulk" limited Frenkel–Poole emission (FPE) or electrode limited Schottky emission (SE). In FPE, emission from "bulk" defects limits charge transport and current density, J_{FPE}, is described by

$$J_{PFE} = \xi_{ox} \exp - \left[q \left\{ \varphi_T - (q\xi_{ox}/\pi\kappa_r\varepsilon_0)^{1/2} \right\} \middle/ kT \right] \quad, \tag{5}$$

where ξ_{ox} is electric field across the dielectric, q is the elementary charge, φ_T is the trap energy depth referenced to the insulator conduction band minimum, k is Boltzmann's constant, T is temperature, ε_0 is the permittivity in vacuum, and κ_r is the electronic component of the dielectric constant (approximately equal to n^2 for ordinary light).

In SE, charge transport is limited by thermal emission over a barrier and current density, J_{SE}, is described by

$$J_{SE} = A^* T^2 \exp - \left[q \left\{ \varphi_B + (q\xi_{ox}/4\pi\kappa_r\varepsilon_0)^{1/2} \right\} \middle/ kT \right] \quad, \tag{6}$$

where A^* is the effective Richardson constant and φ_B is the barrier height at the metal insulator interface.
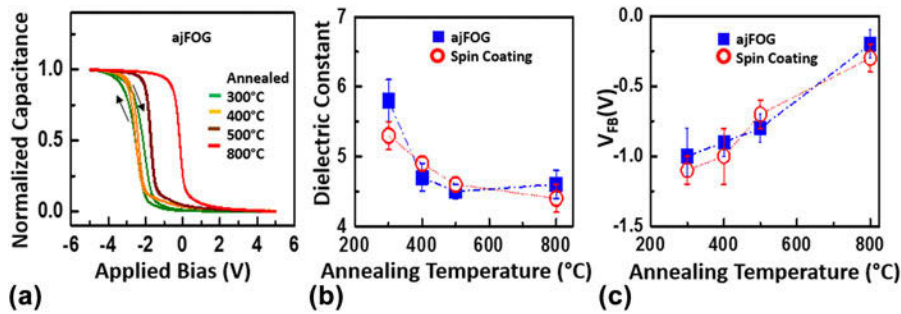
FIG. 7. (a) Representative capacitance versus voltage curves of ajFOG deposited ALPO thin films annealed at various temperatures. (b) Dielectric constant and (c) V_{FB} as a function of annealing temperature for AlPO thin films fabricated using aerosol deposition and spin coating. All films are single layer depositions with $[N]$ = 0.4 M, with $t_w = t_{exp}$ = 120 s for the ajFOG depositions.

To determine whether SE or FPE plays a role in charge transport, $\ln(J)$ versus $\xi_{ox}^{1/2}$ and $\ln(J/\xi_{ox})$ versus $\xi_{ox}^{1/2}$ are plotted in Figs. 6(c) and 6(d), respectively, for both ajFOG and spin-on films annealed at 400 °C. The linear fits in 6(c) suggest that for both films, conduction at low applied field is primarily due to SE, i.e., limited by the thermionic emission of electrons over the metal–insulator barrier. The linear fits in 6(d) suggests that at high field, the charge transport is limited by FPE based transport through defect levels in the bulk of the AlPO. The linearity of conductions plots alone is insufficient to unambiguously assign conduction mechanisms. To increase confidence, we extract κ_r values from the slopes of the linear fits in Figs. 6(c) and 6(d) and compare them with n^2 determined from the ellipsometery data in Fig. 1.[27–29] The linear fitting of SE at low fields and FPE at high fields indicates κ_r values of ~2.0 and 2.5, respectively. Both these values compare favorably to the n^2 value (~2.28) determined from ellipsometery data, increasing confidence in the assignment of SE at low and FPE at high applied electric fields.

The field at which the transition between SE and FPE conduction takes place [Figs. 6(a) and 6(b)] increases with increasing annealing temperature for both deposition techniques, suggesting a reduction in bulk defect levels or perhaps an increase in barrier height due to the formation of an interfacial layer. Above the distinct "knee" in the $\ln(J)$ versus ξ_{ox} plots of the films annealed at 500 and 800 °C, Fowler–Nordheim tunneling, likely through the interfacial layer contributes to conduction as well (see supplementary Fig. S5).

Figure 7(a) shows plots of capacitance versus voltage ($C–V$) as a function of anneal temperature for ajFOG-deposited AlPO thin films. A large clockwise 0.3-eV hysteresis between forward and return sweeps is observed for the samples cured at 300 °C. The voltage sweep and voltage limit dependent hysteresis is likely due to electron trapping and detrapping in switching traps near the interface between the film and the Si substrate. The hysteresis decreases with increased annealing temperature from 0.3 V at 300 °C to 0.1 V at 500 °C, indicating a decrease in the density of these defects. For samples annealed at 800 °C, no hysteresis is observed.

The dielectric constant (κ) of the film stack (AlPO and interfacial layer) is extracted from the maximum capacitance (C_{MAX}) and plotted versus anneal temperature in Fig. 7(b). For both deposition techniques, κ decreases with anneal temperature, saturating at $\kappa \sim 4.5$ at about 500 °C, consistent with previously published results for spin coated AlPO films. As expected, these low frequency dielectric constant values are much higher than the electronic component, κ_r, extracted above.

Figure 7(c) shows experimentally determined V_{FB} as a function of annealing temperature. CV stretch-out is reduced and V_{FB} shifts positive with increasing anneal temperature for both aerosol deposited and spin coated films. The reduction in CV stretch-out indicates a reduction in interface trap density at the insulator–substrate interface. The deviation from the ideal flat band voltage, $V_{FB\text{-}ideal} \approx -0.76$ V, is an indication of fixed charge in the films. The negative shift from $V_{FB\text{-}ideal}$ in the samples processed at 300 and 400 °C indicates positive fixed charge, while the positive shift from $V_{FB\text{-}ideal}$ at 800 °C indicates negative fixed charge near the insulator–substrate interface. After the 500 °C anneal $V_{FB} \simeq V_{FB\text{-}ideal}$, indicating the absence of significant fixed charge near the interface. The similar V_{FB} trend with annealing temperature is another indication that the film quality produced by ajFOG deposition is comparable to films produced via spin coating.

IV. CONCLUSION

An aerosol jet fog deposition system with a unique atomizer composed of two opposing jets located inside the deposition chamber is introduced. The two opposing jets force head-on collisions of precursor streams that shear large droplets into smaller. The orientation and

location of the atomizer allows for the formation of a highly uniform fog, enables the use of low-volatility precursors, and offers the possibility of mixing two different precursors. High-quality AlPO thin films are deposited uniformly on 150-mm Si substrates at room temperature and slightly sub-atmospheric pressure via aerosol deposition in pulse mode using a low volatility aqueous precursor. The thickness of the AlPO film varies less than 4% over the entire wafer with RMS roughness below 0.3 nm. The uniformity of the ajFOG deposited film is comparable to state of the art vacuum deposition techniques. Based on a systematic study of precursor concentration, the characteristic fog settling time, the wait time between fog formation and substrate exposure, fog exposure time, and number of coating cycles, a model of ajFOG deposition is developed that allows accurate prediction of film thickness based on these process parameters. A side by side comparison with spin coated thin films deposited using the same precursor reveals that the ajFOG deposited AlPO thin films have comparable quality in terms of thickness uniformity, density, surface roughness, morphology, electrical properties, and charge transport mechanisms. These results indicate that this new aerosol jet fog deposition technique is a promising option for arbitrarily large-area solution deposition of high-quality thin films at room temperature and slightly sub-atmospheric pressure.

ACKNOWLEDGMENTS

REFERENCES

1. V. Miikkulainen, M. Leskela, M. Ritala, and R.L. Puurunen: Crystallinity of inorganic films grown by atomic layer deposition: Overview and general trend. *J. Appl. Phys.* **113**, 021301 (2013).
2. T.P. Niesen and M.R. De Guire: Review: Deposition of ceramic thin films at low temperatures from aqueous solution. *Solid State Ionics* **151**, 61 (2002).
3. M.G. Kast, L.J. Enman, N.J. Gurnon, A. Nadarajah, and S. Boettcher: Solution-deposited F: SnO_2/TiO_2 as a base-stable protective layer and antireflective coating for microtextured buried-junction H_2-evolving Si photocathodes. *ACS Appl. Mater. Interfaces* **6**, 22830 (2014).
4. K. Norrman, A.G. Siahkali, and N.B Larsen: Studies of spin coated polymer films. *Annu. Rep. Prog. Chem, Sect. C.* **101**, 174 (2005).
5. V.K. Singh, M. Sasaki, J.H. Song, and K. Hane: Techniques for preparing defect-free spray coated resist films on three-dimension micro-electromechanical systems. *Jpn. J. Appl. Phys.* **44**, 2016 (2005).
6. N. Golego, S.A. Studenikin, and M. Cocivera: Properties of dielectric $BaTiO_3$ thin films prepared by spray pyrolysis. *Chem. Mater.* **10**, 2000 (1998).
7. T. Kawaharamura, T. Uchida, M. Sanada, and M. Furuta: Growth and electrical properties of AlO_x grown by mist chemical vapor deposition. *AIP Adv.* **3**, 032135 (2013).
8. M. Huffman: Liquid source misted chemical deposition (LSMCD)—A critical review. *Integr. Ferroelectr.* **10**, 39 (1995).
9. J. Piao, S. Katori, T. Kawaharamura, C. Li, and S. Fujita: Fabrication of silicon oxide thin films by mist chemical vapor deposition method from polysilazane and ozone as source. *Jpn. J. Appl. Phys.* **51**, 090201 (2012).
10. K. Akaiwa and S. Fujita: Electrical conductive corundum-structured α-Ga_2O_3 thin films on sapphire with tin-doping grown by spray-assisted mist chemical vapor deposition. *Jpn. J. Appl. Phys.* **51**, 070203 (2012).
11. H.J. Chung, J.H. Choi, J.Y. Lee, and S.I. Woo: Preparation and electrical properties of $(Ba,Sr)TiO_3$ thin films deposited by liquid source misted chemical deposition. *Thin Solid Film* **382**, 106 (2001).
12. R.N. Rothon: Solution-deposited metal phosphate coatings. *Thin Solid Films* **77**, 149 (1981).
13. S.T. Meyers, T.J. Anderson, D. Hong, C.M. Hung, J.F. Wager, and D.A. Keszler: Solution-processed aluminum oxide phosphatez thin-film dielectrics. *Chem. Mater.* **19**, 4023 (2007).
14. T. Dobbelaere, A.K. Roy, P. Vereecken, and C. Detavernier: Atomic layer deposition of aluminum phosphate based on the plasma polymerization of trimethyl phosphate. *Chem. Mater.* **26**, 6863 (2014).
15. P.G. De Gennes: Wetting: Statics and dynamics. *Rev. Mod. Phys.* **57**, 827 (1985).
16. L.H. Tanner: The spreading of silicone oil drops on horizontal surfaces. *J. Phys. D.: Appl. Phys.* **12**, 1473 (1979).
17. S.L. Cormier, J.D. McGraw, T. Salez, E. Raphaël, and K. Dalnoki-Veress: Beyond Tanner's law: Crossover between spreading regimes of a viscous droplet on an identical film. *Phys. Rev. Lett.* **109**, 154501 (2012).
18. D. Bonn, J. Eggers, J. Indekeu, J. Meunier, and E. Rolley: Wetting and spreading. *Rev. Mod. Phys.* **81**, 739 (2009).
19. Rigaku. PDXL: *Integrated X-ray Powder Diffraction Software* (Rigaku Corporation, Tokyo, Japan, 2010).
20. Bruker: *NanoScope Analysis* (Bruker Corporation, Billerica, MA, 2013).
21. D.K. Schroeder: *Semiconductor Material, and Device Characterization*, 3rd ed. (John Wiley & Sons, Hoboken, NJ, 2005); p. 328.
22. M. Alemayehu, J.E. Davis, M. Jackson, B. Lessig, L. Smith, J.D. Sumega, C. Knutson, M. Beekman, D.C. Johnson, and D.A. Keszler: Tunable dielectric thin films by aqueous, inorganic solution-based processing. *Solid State Sci.* **13**, 2037 (2011).
23. K. Jiang. S.T. Meyers, M.D. Anderson, D.C. Johnson, and D.A. Keszler: Functional ultrathin films and nanolaminates from aqueous solutions. *Chem. Mater.* **25**, 210 (2013).
24. S.W. Smith, W. Wang, D.A. Keszler, and J.F. Conley, Jr.: Solution based prompt inorganic condensation and atomic layer deposition of Al_2O_3 films: A side-by-side comparison. *J. Vac. Sci. Technol., A* **32**, 041501 (2014).
25. J.T. Anderson, W. Wang, K. Jiang, T. Gustafsson, C. Xu, E.L. Gafunkel, and D.A. Keszler: Chemically amplified dehydration of thin oxide films. *ACS Sustainable Chem. Eng.* **3**, 1081 (2015).
26. W. Wang: Ph.D. Dissertation, "Synthesis and characterizations of Aluminum Oxide Based Materials – from Molecules to Devices," Oregon State University, Corvallis, 2013.
27. J. Frenkel: On pre-breakdown phenomena in insulators and electronic semi-conductors. *Phys. Rev.* **54**, 647 (1938).

28. D.S. Jeong, H.B. Park, and C.S. Hwang: Reasons for obtaining an optical dielectric constant from the Poole–Frenkel conduction behavior of atomic-layer-deposited HfO$_2$ films. *Appl. Phys. Lett.* **86**, 072903 (2005).

29. N. Alimardani, S.W. King, B.L. French, C. Tan, B.P. Lampert, and J.F. Conley, Jr.: Investigation of the impact of insulator material on the performance of dissimilar electrode metal-insulator-metal diodes. *J. Appl. Phys.* **116**, 024508 (2014).

Supplementary Material

To view supplementary material for this article, please visit http://dx.doi.org/10.1557/jmr.2016.341. Supporting information including a photograph of the ajFOG deposition system, images of ajFOG films as a function of UV-ozone surface treatment, a thickness map showing air flow thinning of the leading edge during the movement of wafer from the chamber into the load lock, a linear plot of thickness versus wait time for fixed exposure and precursor concentration, and a plot showing Fowler–Nordheim conduction charge transport in aerosol and spin coated AlPO thin films deposited on Si and annealed at 500 and 800 °C is available. (PDF)